A centralized multilayer $LPV/\mathscr{H}_\infty$ control architecture for vehicle's global chassis control, and comparison with a decentralized architecture *

A. Hamdan * **A. Chokor** * **R. Talj** * **M. Doumiati** **

* *Sorbonne universités, Université de technologie de Compiègne, CNRS, Heudiasyc UMR 7253, CS 60 319, 60 203 Compiègne, France.*
** *ESEO-IREENA EA 4642, 10 Bd Jeanneteau, 49100 Angers, France.*

Abstract: This paper deals with the development of Global Chassis Controller where the Active Front steering, Direct Yaw Control and Active Suspensions, are coordinated together in the aim to improve the overall vehicle performance i.e maneuverability, lateral stability and rollover avoidance. The main contribution of this work is the integration of the Active suspension system (AS) in a centralized multilayer control architecture to control the roll angle. A polytopic approach is used to find the $LPV/\mathscr{H}_\infty$ controller where an offline Linear Matrix Inequality (LMI) optimal solver is used to realize the optimality of this controller. The different layers of this architecture are detailed. The proposed $LPV/\mathscr{H}_\infty$ controller is validated by simulation using Matlab/Simulink, and a comparison is done with a decentralized architecture that has been developed in the laboratory, to show the difference in behavior and performance of both strategies of control and the effectiveness of centralized one on the rollover avoidance.

Keywords: Centralized Multilayer Control; $LPV/\mathscr{H}_\infty$; Global Chassis Control; Active Suspensions; Direct Yaw Control; Active Front Steering; decentralized control;

1. INTRODUCTION

Active safety is an important issue considered in intelligent vehicles. According to the "National Highway Traffic Safety Administration (NHTSA)" statistics, human's faults cause almost 90% of road accidents as explained in Rajamani (2012). Advanced Driving Assistance Systems (ADAS) have been developed for several years in order to enhance the stability of road vehicles and to help the driver in maintaining the control of the vehicle under dangerous situations. ADAS systems are formed by several single-actuator approaches that have been proposed and marketed, such as: Electronic Stability Program (ESP) or Direct Yaw Control (DYC) to enhance the vehicle lateral stability; Active Front Steering (AFS) to mainly improve the vehicle maneuverability or lane keeping; and (Semi-) Active Suspensions (AS) to improve comfort, road holding and rollover avoidance [Chokor et al. (2019)].

Many advanced studies are developed in literature to improve the global performance of the vehicle in different driving situations. These studies suggest coordination between several ADAS systems known as Global Chassis Control (GCC). The GCC system deals with the complexity of control problems for Multi-Input-Multi-Output (MIMO) systems. The main objective of the GCC is the coordination between several actuators to improve the vehicle global behavior in terms of maneuverability and lateral stability depending on the driving situation. Many advanced control approaches have been proposed for this issue. The authors in He et al. (2006) applied a decentralized approach where they developed an AFS controller for maneuverability purpose and a DYC controller for lateral stability,

based on sliding mode technique, and then a monitor coordinates between the two controllers according to the driving situations. However, the overall stability of the system cannot be guaranteed in the decentralized approach, especially when the two controllers can be actuated concurrently. In Doumiati et al. (2013), Poussot-Vassal et al. (2009), the authors propose several robust and optimal centralized controllers for the MIMO system based on the LPV/$\mathscr{H}_\infty$ control technique, where the $LPV/\mathscr{H}_\infty$ controller promotes or reduces the steering and braking to enhance maneuverability and lateral stability. With this approach, the overall stability of the system is guaranteed and a polytopic approach is used to actuate the different controllers. However, these controllers were synthesized while disregarding the roll motion; the deduced rollover enhancement was a consequence of the lateral stability control. Authors in Chen et al. (2016), Sename et al. (2013) have presented several centralized $LPV/\mathscr{H}_\infty$ controllers, where AFS, DYC and AS are used to control the lateral and vertical vehicle dynamics. From the other side, authors in Yao et al. (2017), Vu et al. (2017) and Mirzaei and Mirzaeinejad (2017), have used the roll angle and roll rate to control the vehicle load transfer that leads to rollover avoidance. Furthermore, authors deduced lateral stability improvement as a consequence of roll control.

All these interesting research have motivated us to study the control of the vehicle yaw rate, the side slip angle and the roll angle in order to improve the overall vehicle performance. Thus, in our present work, a new centralized multilayer control structure is developed to improve the maneuverability, lateral stability, and rollover avoidance using steering, braking actuators and active suspension system. The global centralized multilayer control architecture is shown in Fig. 1, and is developed later. The paper contributions are as follows:

Fig. 1. Global chassis control architecture

- A new centralized control design, which merges the yaw rate control, the side-slip angle control, and the roll control, in one single centralized controller to maintain internal stability when switching between maneuverability, lateral stability and rollover avoidance objectives.
- A comparison between the proposed controller, and a decentralized one, developed in the laboratory and based on sliding mode technique.

The paper structure is as follows: Section 2 exposes the extended bicycle model of the vehicle based on the combination of the coupled lateral (yaw and side-slip) and roll motions. In Section 3, the proposed centralized control architecture is detailed, starting by a presentation of the MIMO $LPV/\mathscr{H}_\infty$ as a model-based controller. Then we pass to detail the control objectives represented as variable-weighted filters, to finally develop the $LPV/\mathscr{H}_\infty$ controller which guarantees $\mathscr{H}_\infty$ performances between the exogenous inputs and the controlled variables, based on offline Linear Matrix Inequalities LMI optimization, in the framework of the polytopic approach. A decentralized architecture developed in the laboratory is presented briefly in this section. Simulation validation of the proposed approach is reported in Section 4. Finally, the conclusions and the perspectives of this work are given in Section 5.

2. VEHICLE MODEL

The vehicle is a group of interconnected mechanical and electrical systems that make the vehicle behavior nonlinear. The ADAS systems such as AFS (Active Front Steering), active suspensions, differential braking, etc, improve the vehicle's performance (lateral motion, yaw motion, roll motion, etc.). A complete nonlinear vehicle model has been developed in Chokor et al. (2016). However, this model is a nonlinear model that does not respond to the formulation of control problems. For this reason, a linear simplified LTI vehicle model is used to develop the GCC controller. This LTI model is a coupled yaw-lateral-roll linear vehicle model, inspired from literature [Vu et al. (2017)], and is given by the following equations of *"Plant P"*:

$$PlantP: \begin{cases} I_z\ddot{\psi} = F_{yf}l_f + F_{yr}l_r + I_{xz}\ddot{\theta} + M_z + M_{d,\psi}, \\ M\mathrm{V}(\dot{\beta}+\dot{\psi}) = F_{yf} + F_{yr} + M_s h_\theta \ddot{\theta} + F_{d,y}, \\ (I_x + M_s h_\theta^2)\ddot{\theta} = M_s h_\theta \mathrm{V}(\dot{\beta}+\dot{\psi}) + (M_s g h_\theta - K_\theta)\theta \\ \qquad\qquad - C_\theta \dot{\theta} + M_{d,\theta}, \end{cases} \tag{1}$$

where the vehicle parameters and variables are given in Table 1. F_{yf} represents the lateral force of the front left and right tires

Table 1. Parameters Values for Simulation

Symbols	Description	Parameters values
$\dot{\psi}$	Vehicle yaw rate	$[rad/s]$
β	Vehicle side slip angle at CG	$[rad]$
θ	Sprung mass roll angle	$[rad]$
F_{yi}	Lateral forces at the i axle	$[N]$
δ_d	Driver steering angle	$[rad]$
V	Vehicle speed	$[m/s]$
I_x	Roll moment of inertia of sprung mass	$534\ [kg.m^2]$
I_z	Vehicle yaw moment of inertia	$1970\ [kg.m^2]$
I_{xz}	Vehicle yaw-roll product of inertia	$743\ [kg.m^2]$
t_f	Half front track	$0.773\ [m]$
t_r	Half rear track	$0.773\ [m]$
l_f	Wheelbase to the front	$1.0385\ [m]$
l_r	Wheelbase to the rear	$1.6015\ [m]$
h_θ	Sprung mass roll arm	$0.27\ [m]$
M_s	Sprung mass	$1126.4\ [kg]$
C_f, C_r	Front, rear tire cornering stiffness	$76776\ [N/rad]$
K_θ	Roll suspension angular stiffness	$30000\ [N.m/s]$
C_θ	Roll suspension angular damper	$10000\ [N.m/s]$
g	Gravity constant	$9.81\ [m/s^2]$
μ	Road adherence coefficient	dry surface= 1 $[-]$

merged together at the center of the front axle. Similarly, F_{yr} is noted for the rear axle. F_{yf} and F_{yr} are given as:

$$\begin{aligned} F_{yf} &= \mu C_f \alpha_f, \\ F_{yr} &= \mu C_r \alpha_r, \end{aligned} \tag{2}$$

and the tires slip angles as:

$$\begin{aligned} \alpha_f &= -\beta - \frac{l_f \dot{\psi}}{V} + \delta_t, \\ \alpha_r &= -\beta + \frac{l_r \dot{\psi}}{V}. \end{aligned} \tag{3}$$

By substituting (3) in (2), and then by substituting (2) in (1), the state space representation of the *Plant P* can be represented in (4) (given next page), where $X = [\dot{\psi}, \beta, \theta, \dot{\theta}]^T$ is the state vector, $U = [\delta_c, Mz]^T$ is the vector of control inputs, $D = [M_{d,\psi}, F_{d,y}, M_{d,\theta}]^T$ is the vector of exogenous inputs. Noting that the matrix $A \in I\!R^{4\times4}$, and the input matrices $B_u \in I\!R^{4\times3}$ and $B_d \in I\!R^{4\times3}$. In real time control, the output controlled variables $\dot{\psi}$ and $\dot{\theta}$ are given at the center of gravity (CG) of the vehicle by a gyrometer; θ is estimated by a simple time integration from $\dot{\theta}$ and could be directly delivered from the Inertial Measurement Unit (IMU) if available. The other states, side-slip angle β and its velocity $\dot{\beta}$, could be calculated by an estimation. To do that, many observer approaches that deal with the real time implementation and vehicle dynamics have been presented in the literature, e.g. an observer based on Extended Kalman Filter EKF as proposed in Chen et al. (2016).

It should be noticed that the *"bicycle model"* used in the control layer of Fig. 1 is presented in Rajamani (2012) and is given in (5):

$$\begin{pmatrix} \ddot{\psi}_{ref} \\ \dot{\beta}_{ref} \end{pmatrix} = \begin{bmatrix} -\mu\frac{l_f^2 c_f + l_r^2 c_r}{I_z V_x} & \mu\frac{l_r c_r - l_f c_f}{I_z} \\ -1 + \mu\frac{l_r c_r - l_f c_f}{M V_x^2} & -\mu\frac{c_f + c_r}{M V_x} \end{bmatrix} \begin{pmatrix} \dot{\psi}_{ref} \\ \beta_{ref} \end{pmatrix} + \begin{bmatrix} \mu\frac{l_f c_f}{I_z} \\ \mu\frac{c_f}{M V_x} \end{bmatrix}\delta_d, \quad (5)$$

where δ_d is the driver steer angle on the front wheels, $\dot{\psi}_{ref}$ is the desired reference yaw rate, β_{ref} is the corresponding side slip angle, and V_x is the vehicle longitudinal speed, considered as a varying parameter. For security reasons, the authors in Rajamani (2012) propose to saturate β_{ref} and $\dot{\psi}_{ref}$ below a threshold, as described in (6):

$$\begin{aligned} &\mid \dot{\psi}_{ref} \mid \leq \mid \frac{0.85\mu g}{V_x} \mid \\ &\beta_{ref} = \arctan(0.02\mu g) \end{aligned} \tag{6}$$

$$\dot{X} = \begin{bmatrix} \ddot{\psi} \\ \dot{\beta} \\ \dot{\theta} \\ \ddot{\theta} \end{bmatrix} = \underbrace{\begin{pmatrix} a_{11} & a_{12} & a_{13} & a_{14} \\ a_{21} & a_{22} & a_{23} & a_{24} \\ 0 & 0 & 0 & 1 \\ a_{41} & a_{42} & a_{43} & a_{44} \end{pmatrix}}_{A} \underbrace{\begin{bmatrix} \dot{\psi} \\ \beta \\ \theta \\ \dot{\theta} \end{bmatrix}}_{X} + \underbrace{\begin{pmatrix} b_{u,11} & b_{u,12} & b_{u,13} \\ b_{u,21} & b_{u,22} & b_{u,23} \\ 0 & 0 & 0 \\ b_{u,41} & b_{u,42} & b_{u,43} \end{pmatrix}}_{B_u} \underbrace{\begin{bmatrix} \delta_d + \delta_c \\ M_z \\ M_\theta \end{bmatrix}}_{U} + \underbrace{\begin{pmatrix} b_{d,11} & 0 & 0 \\ 0 & b_{d,22} & 0 \\ 0 & 0 & 0 \\ 0 & 0 & b_{d,43} \end{pmatrix}}_{B_d} \underbrace{\begin{bmatrix} M_{d,\dot{\psi}} \\ F_{d,y} \\ M_{d,\theta} \end{bmatrix}}_{D};$$

$$y = X. \tag{4}$$
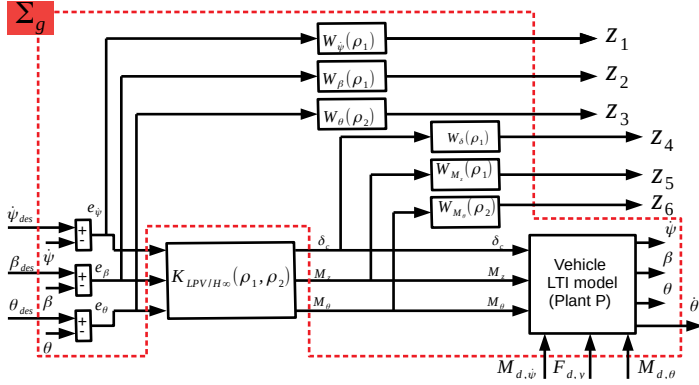
Fig. 2. Control layer architecture

3. GLOBAL CHASSIS CONTROL

3.1 Centralized Control Architecture:

In this subsection, we present a detailed synthesis of the centralized multi-layer global chassis control architecture of Fig. 1, based on the $LPV/\mathscr{H}_\infty$ theory. In the control layer, the output variables i.e the vehicle yaw rate $\dot{\psi}$, the side-slip angle β, and the suspended mass roll θ are controlled and optimized together through an optimal $MIMO\ LPV/\mathscr{H}_\infty$ centralized controller, in order to enhance the vehicle maneuverability, the lateral stability and the rollover avoidance. $\dot{\theta}$ is an exogenous output. The desired states ψ_{ref}, and β_{ref} are given in (5). In addition, ρ_1 and ρ_2 are two time-varying scheduling gains/parameters to organize the objectives of the $MIMO\ LPV/\mathscr{H}_\infty$ controller. A decision layer is developed to control the situation of the vehicle; it sends the values of scheduling parameters, based on two criteria: lateral stability (SI) and load transfer ratio (LTR), discussed later. The actuator layer contains AFS, DYC and AS; it generates the physical inputs to vehicle system.

i) Control layer:
The architecture of the control layer is presented in Fig. 2. It contains the controller $K_{LPV/\mathscr{H}_\infty}(\rho_1,\rho_2)$ to be developed, the generalized plant $\sum_g$, where ρ_1 and ρ_2 are two endogenous weighted parameters determined by the decision-making monitor according to the driving situations and the LTI model (Plant P) used in the synthesis of this controller. The inputs of $K_{LPV/\mathscr{H}_\infty}(\rho_1,\rho_2)$ controller are the errors between the desired states and the actual ones of the yaw rate $e_{\dot{\psi}}$, the side-slip angle e_β, and the roll angle e_θ. Noting that the actual yaw rate $\dot{\psi}$, side slip angle β, and roll angle θ are the outputs variables to be controlled and they are delivered from the LTI model (Plant P). The inputs of the Plant P are the AFS angle δ_c, the moment M_z around z axis (generated by the DYC) and the moment M_θ around the roll axis (generated by the AS); $M_{d,\dot{\psi}}$, $F_{d,y}$, and $M_{d,\theta}$ are the disturbances related to the road status and weather conditions like wind (exogenous inputs). $W_{\dot{\psi}}(\rho_1)$, $W_\beta(\rho_1)$, $W_\theta(\rho_2)$, $W_\delta(\rho_1)$, $W_{M_z}(\rho_1)$ and $W_{M_\theta}(\rho_2)$ are the weighting functions de-

termined in order to define the performance objectives Z_1, Z_2, and Z_3 and the actuator limitations Z_4, Z_5 and Z_6. The general form of these functions (see [Doumiati et al. (2014)]) depends on the simulated vehicle and integrated actuators:

- $W_{\dot{\psi}}(\rho_1)$ weights the yaw rate signal:

$$W_{\dot{\psi}}(\rho_1) = \rho_1 \frac{s/M_1 + 2\pi f_1}{s + 2\pi f_1 T_1}, \tag{7}$$

where M_1 is the margin of robustness, and T_1 is the tolerated tracking error on $e_{\dot{\psi}}$. $W_{\dot{\psi}}(\rho_1)$ is defined to diminish the yaw rate error in the range of frequencies lower than the roll-off frequency f_1 where the vehicle operates [Heißing and Ersoy (2010)]. $W_{\dot{\psi}}(\rho_1)$ is linearly parametrized by the varying parameter ρ_1, where $\rho_1 \in \left\{ \underline{\rho_1} \le \rho \le \overline{\rho_1} \right\}$ (with $\underline{\rho_1}$ and $\overline{\rho_1}$ are constants representing the lower and higher values of ρ_1). When $\rho_1 = \overline{\rho_1}$, maneuverability purpose is improved and the performance objective $e_{\dot{\psi}}$ is penalized, on the contrary, when $\rho_1 = \underline{\rho_1}$, $e_{\dot{\psi}}$ is relaxed and the lateral stability becomes a priority objective to be realized.

- $W_\beta(\rho_1)$ weights the side slip angle:

$$W_\beta(\rho_1) = \frac{1}{\rho_1} \frac{s/M_2 + 2\pi f_2}{s + 2\pi f_2 T_2}. \tag{8}$$

M_2, T_2 and f_2 have similar definitions as M_1, T_1 and f_1. $W_\beta(\rho_1)$ is designed similarly to $W_{\dot{\psi}}(\rho_1)$. $W_\beta(\rho_1)$ is inversely dependent on the varying parameter ρ_1. This is because the lateral stability is more penalized than maneuverability in critical situations. This issue is detailed later in the decision layer.

- $W_\theta(\rho_2)$ weights the roll angle according to a scheduling parameter ρ_2:

$$W_\theta(\rho_2) = \rho_2 \frac{s/M_3 + 2\pi f_3}{s + 2\pi f_3 T_3}. \tag{9}$$

M_3, T_3 and f_3 have similar meanings as M_1, T_1 and f_1. $W_\theta(\rho_2)$ is linearly parametrized by the varying parameter ρ_2, where $\rho_2 \in \left\{ \underline{\rho_2} \le \rho_2 \le \overline{\rho_2} \right\}$ ($\underline{\rho_2}$ and $\overline{\rho_2}$ are constants representing the lower and higher values of ρ_2). When $\rho_2 = \overline{\rho_2}$, the performance objective e_θ is penalized and the rollover avoidance is a priority. On the contrary, when $\rho_2 = \underline{\rho_2}$, e_θ is relaxed and rollover is not a risk.

- $W_\delta(\rho_1)$ weights the steering control signal, δ_c:

$$
\begin{aligned}
W_\delta(\rho_1) &= \left(\frac{1}{\rho_1}\right) G_\delta^0 \frac{(s/2\pi f_4 + 1)(s/2\pi f_5 + 1)}{(s/\alpha 2\pi f_5 + 1)^2}, \\
G_\delta^0 &= \frac{(\Delta_f/\alpha 2\pi f_5 + 1)^2}{(\Delta_f/2\pi f_4 + 1)(\Delta_f/2\pi f_5 + 1)}, \\
\Delta_f &= 2\pi(f_4 + f_5)/2,
\end{aligned}
\tag{10}
$$

where f_4 and f_5 are the lower and upper limits of the filter bandwidth $[f_4, f_5]$. This filter is proposed to force the active steering system to act in this range $[f_4, f_5]$. Otherwise, this filter ensures the activation of steering system below the cutof frequency (f_5) and above the driver ones (f_4) (see [Doumiati et al. (2014)]). Note that steering system is promoted to enhance the maneuverability when $\rho_1 = \overline{\rho_1}$ and vice versa.

- $W_{M_z}(\rho_1)$ weights the braking, M_z:

$$W_{M_z}(\rho_1) = \rho_1 10^{-6} \frac{s/(2\pi f_6)+1}{s/(\kappa 2\pi f_6)+1}, \tag{11}$$

where f_6 is the braking actuator cut-off frequency and κ to treat the braking actuator limitations (see [Doumiati et al. (2013)]). When $\rho_1 = \overline{\rho_1}$, the braking input is penalized, on the contrary, the braking control signal is relaxed when $\rho_1 = \underline{\rho_1}$. This design depends on the vehicle lateral stability.

- $W_{M_\theta}(\rho_2)$ weights the suspensions M_θ:

$$W_{M_\theta}(\rho_2) = (\frac{1}{\rho_2}) 10^{-4} \frac{s/(2\pi f_7)+1}{s/(\kappa 2\pi f_7)+1}, \tag{12}$$

where f_7 is the cut-off frequency and κ determines the limitation of suspension system. When $\rho_2 = \underline{\rho_2}$, the suspension system is penalized, however, the suspension system is relaxed when $\rho_2 = \overline{\rho_2}$ (case of rollover risk is detected). Note that we didn't consider the actuators' constraints in this control layer. However, the control inputs are filtered by using the weights above and the actuators' models in the actuator layer. In addition, the tuning of the gains ρ_1 and ρ_2 respects the time response of the actuators.

After determining the subsystems of Fig. 2, $\mathscr{H}_\infty$ control technique is applied in order to minimize the controlled outputs Z_1, Z_2, Z_3, Z_4, Z_5 and Z_6 in presence of disturbances $M_{d,\psi}, F_{d,y}, M_{d,\theta}$ and exogenous inputs $\psi_{des}, \beta_{des}, \theta_{des}$. More information about the optimal $LPV/\mathscr{H}_\infty$ theory is presented in Sename et al. (2013) and Gu et al. (2005).

A "*sysic*" Matlab function (Robust Control Toolbox) is used to make the interconnection between $\sum_g$ subsystems. The generalized plant $\sum_g$ is *LPV* [Apkarian et al. (1995)], given as following as:

$$\Sigma_g(\rho) : \begin{bmatrix} \dot{x} \\ z \\ y \end{bmatrix} = \begin{bmatrix} A(\rho) & B_1(\rho) & B_2(\rho) \\ C_1(\rho) & D_{11}(\rho) & D_{12}(\rho) \\ C_2 & D_{21} & 0 \end{bmatrix} \begin{bmatrix} x \\ w \\ u \end{bmatrix}, \tag{13}$$

where $\rho = \{\rho_1, \rho_2\}$, x is the vector of states variables of *Plant P* and of the weighting functions, $u = [\delta_c, M_z, M_\theta]^T$ represents the control inputs, $w = [\psi_{des}, \beta_{des}, \theta_{des}, M_{d,\psi}, F_{d,y}, M_{d,\theta}]^T$ is the exogenous input vector, $y = [\psi, \beta, \theta]^T$ is the measurement vector fed-back to the controller, $y_e = [\dot{\theta}]^T$ is the exogenous output, and $z = [Z_1, Z_2, Z_3, Z_4, Z_5, Z_6]^T$ is the controlled output vector. Note that the matrices B_2, and D_{12} depend on ρ, which is not consistent with the requirements of $\mathscr{H}_\infty$ synthesis for polytopic systems. Some filters on the control input have been used to solve this problem [Apkarian and Gahinet (1995)].

Problem resolution: LMI based LPV/$\mathscr{H}_\infty$:
The problem of $LPV/\mathscr{H}_\infty$ is to find the controller $K_{LPV/\mathscr{H}_\infty}(\rho_1, \rho_2)$, scheduled by the parameters ρ_1 and ρ_2, such that:

$$K_{LPV/\mathscr{H}_\infty}(\rho) : \begin{bmatrix} \dot{x}_c \\ u \end{bmatrix} = \begin{bmatrix} A_c(\rho) & B_c(\rho) \\ C_c(\rho) & 0 \end{bmatrix} \begin{bmatrix} x_c \\ y \end{bmatrix}, \tag{14}$$

This controller aims to minimize the $\mathscr{H}_\infty$ norm of the closed-loop *LPV* system established by the equations (13) and (14). Several approaches exist in the literature to solve this problem such as: polytopic, gridding and Linear Fractional Transformation LFT [Zin (2005)]. In our work, a polytopic approach [see Scherer et al. (1997)] has been used for controller synthesis. Applying the Bounded Real Lemma (BRL) extended to LPV systems and after a change of basis presented in [Scherer et al. (1997)], a non conservative *LMI* is formulated in (15) and a Semi-Definite Program (SDP) has been applied to solve these inequalities equations (see [Doumiati et al. (2013)]), while minimizing γ for $\rho \in \Omega = [\underline{\rho_1}, \overline{\rho_1}] X [\underline{\rho_2}, \overline{\rho_2}]$. The aim of polytopic approach is to find the $\widetilde{A}(\rho)$, $\widetilde{B}(\rho)$ and $\widetilde{C}(\rho)$ by using

a common Lyapunov function i.e $X(\rho) > 0$ and $Y(\rho) > 0$ at each vertex of the polytope function of $\rho \in \Omega$. Noting that the number of vertex is 4 (2^n) where n is the number of exogenous parameters. Thus, the solution is given by the resolution of system (16) at each vertex of the convex hull Ω $\left\{ \omega_1 = (\underline{\rho_1}, \underline{\rho_2}), \omega_2 = (\overline{\rho_1}, \underline{\rho_2}), \omega_3 = (\underline{\rho_1}, \overline{\rho_2}), \omega_4 = (\overline{\rho_1}, \overline{\rho_2}) \right\}$:

$$\begin{cases} C_c(\rho) = \widetilde{C}(\rho) M(\rho)^{-T} \\ B_c(\rho) = N(\rho)^{-1} \widetilde{B}(\rho) \\ A_c(\rho) = N(\rho)^{-1} (\widetilde{A}(\rho) - Y(\rho)A(\rho)X(\rho) - N(\rho)B_c(\rho). \\ \quad C_2 X(\rho) - Y(\rho)B_2(\rho)C_c(\rho)M(\rho)^{-T})M(\rho)^{-T} \end{cases} \tag{16}$$

where $M(\rho)N(\rho)^T = I - X(\rho)Y(\rho)$ with $M(\rho)$ and $N(\rho)$ are given by the user. More details about the computation solution have been presented in [Scherer et al. (1997)]. Therefore, referring to the polytopic approach, the final controller $K_{LPV/\mathscr{H}_\infty}(\rho_1, \rho_2)$ is the summation of each convex controller calculated on each vertex of polytope [Apkarian et al. (1995)]:

$$K_{LPV/\mathscr{H}_\infty}(\rho_1, \rho_2) = \alpha_1 K_{\mathscr{H}_\infty}(\omega_1) + \alpha_2 K_{\mathscr{H}_\infty}(\omega_2) \\ + \alpha_3 K_{\mathscr{H}_\infty}(\omega_3) + \alpha_4 K_{\mathscr{H}_\infty}(\omega_4), \tag{17}$$

where $\sum_{i=1}^{i=4} \alpha_i(\rho_1, \rho_2) = 1$; $\alpha_i(\rho_1, \rho_2) > 0$. Depending on the driving situation given in Fig. 3, the different polytopic coordinates $\alpha_i(\rho_1, \rho_2)$ weight the controller on each vertex in order to build the final controller of our system. They are calculated by using the Matlab function "*polydec*" (Robust Control Toolbox):

$$\alpha_1 = \frac{\overline{\rho_1}-\rho_1}{\overline{\rho_1}-\underline{\rho_1}} . \frac{\overline{\rho_2}-\rho_2}{\overline{\rho_2}-\underline{\rho_2}}; \qquad \alpha_3 = \frac{\overline{\rho_1}-\rho_1}{\overline{\rho_1}-\underline{\rho_1}} . \frac{\rho_2-\underline{\rho_2}}{\overline{\rho_2}-\underline{\rho_2}};$$

$$ \tag{18}$$

$$\alpha_2 = \frac{\rho_1-\underline{\rho_1}}{\overline{\rho_1}-\underline{\rho_1}} . \frac{\overline{\rho_2}-\rho_2}{\overline{\rho_2}-\underline{\rho_2}}; \qquad \alpha_4 = \frac{\rho_1-\underline{\rho_1}}{\overline{\rho_1}-\underline{\rho_1}} . \frac{\rho_2-\underline{\rho_2}}{\overline{\rho_2}-\underline{\rho_2}}.$$

ii) Decision Layer:
The decision layer is dedicated to adjust the controller achievements according to the driver situations. This layer delivers the two endogenous parameters ρ_1 and ρ_2 based on two criteria, lateral stability (*SI*) and load transfer ratio (*LTR*). Before the determination of these parameters, let us introduce the definition of these important criteria in the decision of the driver situation.

-"*Lateral Stability Index*" SI:
The lateral stability index *SI* determines the orientation of the vehicle depending on the speed vector at the *CG*, and its rate of change. *SI* is given as (see [Chen et al. (2016)]):

$$SI = |c_1\beta + c_2\dot{\beta}|, \tag{19}$$

where c_1 and c_2 are estimated w.r.t the vehicle parameters and the shape of the road. *SI* varies between 0 and 1. An analysis of the driver situation is done depending on *SI*. For example, when $SI \leq \underline{SI}$ the vehicle is in normal driving situations. Therefore, the AFS is activated to enhance the maneuverability and the lateral stability in the moderate range of *SI*, and the DYC is penalized. In the contrary, when *SI* increases progressively and becomes closer to $\overline{SI}$ limit ($SI \geq \overline{SI}$), a lateral stability enhancement is needed and the DYC is activated. Referring to this analysis, the scheduled gain ρ_1 is designed to provide the $LPV/\mathscr{H}_\infty$ controller, the necessary information about the weights to be pushed or attenuated. The relation between ρ_1 and *SI* is given through a "*sigmoid*" function (20) (see Fig. 4.a) that guarantees a continuous and smooth variation of ρ_1.

$$\rho_1 = \overline{\rho_1} - \frac{\overline{\rho_1} - \underline{\rho_1}}{1 + e^{-\frac{8}{\overline{SI}-\underline{SI}}(SI - \frac{\overline{SI}+\underline{SI}}{2})}}. \tag{20}$$

$$\begin{bmatrix} A(\rho)X + XA(\rho)^T + B_2\widetilde{C}(\rho) + \widetilde{C}(\rho)^T B_2^T & (*)^T & (*)^T & (*)^T \\ \widetilde{A}(\rho) + A(\rho)^T & YA(\rho) + A(\rho)^T Y + \widetilde{B}(\rho)C_2 + C_2^T\widetilde{B}(\rho)^T & (*)^T & (*)^T \\ B_1(\rho)^T & B_1(\rho)^T Y + D_{21}^T\widetilde{B}(\rho)^T & -\gamma I & (*)^T \\ C_1(\rho)X + D_{12}\widetilde{C}(\rho) & C_1(\r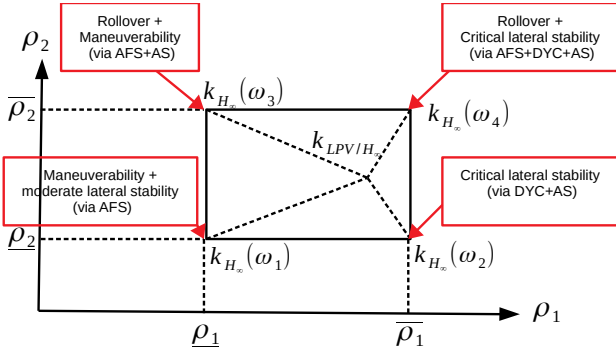ho) & D_{11}(\rho) & -\gamma I \end{bmatrix} < 0 \text{ and } \begin{bmatrix} X(\rho) & I \\ I & Y(\rho) \end{bmatrix} > 0.$$

(15)

Fig. 3. Controller - Polytopic approach
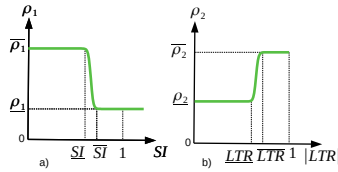
Fig. 4. Scheduling parameters

-"*Load Transfer Ratio*" *LTR*:
The load transfer ratio *LTR* reflects vertical charge transfer from the inside to the outside wheels w.r.t the corner (turn). *LTR* is function of the roll angle, its rate of change and the lateral acceleration and is given by an estimation of different parameters, as follows (see [Rajamani (2012)]):

$$LTR = r_1\theta + r_2\dot{\theta} + r_3 a_y,$$ (21)

where r_1, r_2 and r_3 are estimated depending on the vehicle parameters. *LTR* varies between -1 and 1. When, $LTR \le \underline{LTR}$, no rollover risk is detected and the suspension system is deactivated, until that *LTR* increases and becomes $LTR \ge \overline{LTR}$, so a rollover should be prevented and the active suspension system is promoted. To do this issue, a "*sigmoid*" function (22) (see Fig. 4.b) is given to illustrate the relation between ρ_2 and $|LTR|$:

$$\rho_2 = \underline{\rho_2} + \frac{\overline{\rho_2} - \underline{\rho_2}}{1 + e^{-\frac{8}{\overline{LTR} - \underline{LTR}}(|LTR| - \frac{\overline{LTR} + \underline{LTR}}{2})}}.$$ (22)

iii) Actuator layer:
The actuator layer includes the different actuators used to generate the physical inputs of the system. In our work, AFS, DYC and AS have been used to provide these inputs. The AFS is an electrical motor which provides the added steering angle δ_c^a. In order to ensure that the AFS actuator is able to provide the added steering angle demanded by the controller δ_c, the AFS is modeled as follows:

$$\dot{\delta}_c^a = 2\pi f_5(\delta_c - \delta_c^a),$$ (23)

where δ_c^a follows δ_c, f_5 is the actuator cut-off frequency. This actuator is bounded between $\left[-\delta_{c,max}^a, +\delta_{c,max}^a\right]$, with $\delta_{c,max}^a$ the maximum amount of steering angle that can be added by the AFS actuator.

In the same way, the DYC moment M_z can be realized by applying a braking torque on the rear wheels of radius r [Doumiati et al. (2014)]. The applied braking torque is given as follows:

$$\begin{cases} \begin{cases} Tb_{rr} = -\frac{2*M_z*r}{t_r}, & if\ M_z \le 0, \\ Tb_{lr} = 0, \end{cases} \\ \begin{cases} Tb_{lr} = \frac{2*M_z*r}{t_r}, & if\ M_z > 0, \\ Tb_{rr} = 0, \end{cases} \end{cases}$$ (24)

where Tb_{lr} and Tb_{rr} are the left and right differential braking torque respectively. A simple model for the electro mechanical braking (EMB) actuator is used. The EMB actuator is modeled as:

$$\dot{T}_{b,rj}^a = 2\pi f_6(T_{b,rj} - T_{b,rj}^a),$$ (25)

where $T_{b,rj}^a$ tracks $T_{b,rj}$, f_6 is the actuator cut-off frequency. This actuator control is bounded between $[0, T_{b,max}^a]$, where $T_{b,max}^a$ is the saturation of the EMB actuator.

Finally, the M_θ moment is achievable by applying the active suspensions force-actuators on each wheel. These forces are given in the following form (see [Chokor et al. (2017)]):

$$\begin{cases} U_{fl} = 0.5\frac{l_r}{l_f+l_r}\frac{M_\theta}{t_f}, \\ U_{fr} = -0.5\frac{l_r}{l_f+l_r}\frac{M_\theta}{t_f}, \\ U_{rl} = 0.5\frac{l_f}{l_f+l_r}\frac{M_\theta}{t_r}, \\ U_{rr} = -0.5\frac{l_f}{l_f+l_r}\frac{M_\theta}{t_r}. \end{cases}$$ (26)

3.2 Decentralized Control Architecture:

The global decentralized multilayer control architecture of Fig. 5 is presented briefly in this subsection. This architecture has been developed in the frame of global chassis control in the laboratory and is used to compare the results between the centralized and decentralized architecture [Chokor et al. (2019)]. This decentralized sliding mode approach is chosen for the comparison purpose, because it represents the industrial state of the art and it is robust in case of system's uncertainty, disturbance and possible sensor faults. The main difference between the two architectures is in the control layer. Thus, the output variables i.e the vehicle yaw rate ψ, the side-slip angle β, and the suspended mass roll θ are controlled independently by using the single-input, single-output controller based on the Super-Twisting Sliding Mode (STSM) technique. Let us introduce an overview of the theory of Super-Twisting Sliding Mode. The STSM is a robust control technique that forces the states of the system to reach a sliding surface during a finite time (convergence phase) and to stay on this surface (sliding phase) in presence of perturbations.
Consider the second order system given as:

$$\ddot{x} = f(X,t) + g(X,t)u(t)$$ (27)

where $X = [x, \dot{x}]^T \in \Re^2$ is the state vector, u is the control input, and f, g are continuous functions. X_{des} is the desired state of X with $X_{des} = [x_{des}, \dot{x}_{des}]^T \in \Re^2$. The error vector is given by
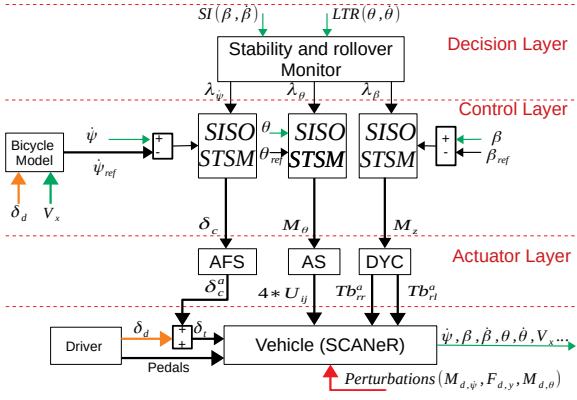
Fig. 5. Decentralized global chassis control architecture

$E = X - X_{des} = [e, \dot{e}]^T \in \Re^2$ where $e = x - x_{des}$ and $\dot{e} = \dot{x} - \dot{x}_{des}$. Therefore, a sliding variable s with relative degree $r = 1$ w.r.t the control input, is defined as:

$$s = \dot{e} + k\,e, \qquad (28)$$

The second order derivative of s is:

$$\ddot{s}(s,t) = \Phi(s,t) + \xi(s,t)\dot{u}(t) \qquad (29)$$

where $\Phi(s,t)$ and $\xi(s,t)$ are the unknown bounded signals.
The goal of the Super-Twisting algorithm is to enforce the sliding variable s to converge to zero ($s = 0$) in finite time. Assume that there exist positive constants S_0, b_{min}, b_{max}, C_0, U_{max} verifying for all $x \in \Re^n$ and $|s(x,t)| < S_0$:

$$\begin{cases} |u(t)| \leq U_{max} \\ |\Phi(s,t)| < C_0 \\ 0 < b_{min} \leq |\xi(s,t)| \leq b_{max} \end{cases} \qquad (30)$$

Thus, the control input based on the Super-Twisting Sliding Mode algorithm, is given as:

$$u(t) = u_1 + u_2 \begin{cases} u_1 = -\alpha_1 |s|^{\tau} \text{sign}(s), \ \ \tau \in]0, 0.5] \\ \dot{u}_2 = -\alpha_2 \text{sign}(s) \end{cases} \qquad (31)$$

α_1 and α_2 are positive gains. The following conditions guarantee the finite time convergence:

$$\begin{cases} \alpha_1 \geq \sqrt{\dfrac{4C_0(b_{max}\alpha_2 + C_0)}{b_{min}^2(b_{min}\alpha_2 - C_0)}} \\ \alpha_2 > \dfrac{C_0}{b_{min}} \end{cases} \qquad (32)$$

The analysis of convergence is presented in Utkin (2013). An approximation function $\frac{s}{|s|+\varepsilon}$ is used to smooth the $sign(s)$ function, where $\varepsilon > 0$.
Let us define the three sliding variables for the three decentralized controllers as follows:

$$\begin{aligned} s_{\dot{\psi}} &= e_{\dot{\psi}} = \dot{\psi} - \dot{\psi}_{ref}, \\ s_{\beta} &= e_{\beta} = \beta - \beta_{ref}, \\ s_{\theta} &= \dot{e}_{\theta} + k_{\theta}\,e_{\theta} = (\dot{\theta} - \dot{\theta}_{ref}) + k_{\theta}(\theta - \theta_{ref}), \end{aligned} \qquad (33)$$

The sliding variables $s_{\dot{\psi}}$, s_{β} and s_{θ} have a relative degree equal to one w.r.t δ_c, M_z and M_{θ} respectively. Thus, in order to converge these variables to zero and the controlled states follow the desired ones, and based on the above discussion, the control inputs of AFS, DYC and AS applied to the system, are given by:

$$\begin{aligned} \delta_c &= -\alpha_{\delta,1}|s_{\dot{\psi}}|^{\tau_\delta} sign(s_{\dot{\psi}}) - \alpha_{\delta,2}\int_0^t sign(s_{\dot{\psi}})d\tau, \\ M_z &= -\alpha_{M_z,1}|s_{\beta}|^{\tau_{M_z}} sign(s_{\beta}) - \alpha_{M_z,2}\int_0^t sign(s_{\beta})d\tau \\ M_{\theta} &= -\alpha_{M_{\theta},1}|s_{\theta}|^{\tau_{M_\theta}} sign(s_{\theta}) - \alpha_{M_{\theta},2}\int_0^t sign(s_{\theta})d\tau, \end{aligned} \qquad (34)$$

where $\alpha_{\delta,i}$, $\alpha_{M_z,i}$ and $\alpha_{M_{\theta},i}$ with $i = [1, 2]$, are positive constants satisfying the conditions in (32). τ_δ, τ_{M_z} and τ_{M_θ} are constants
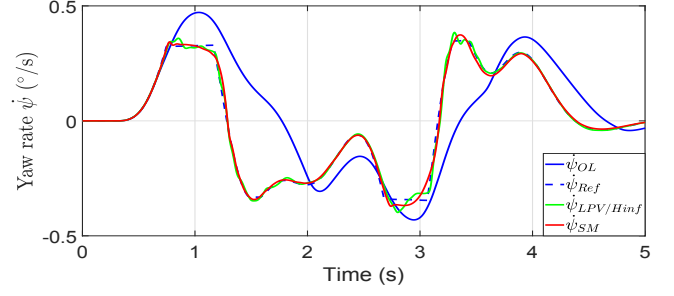
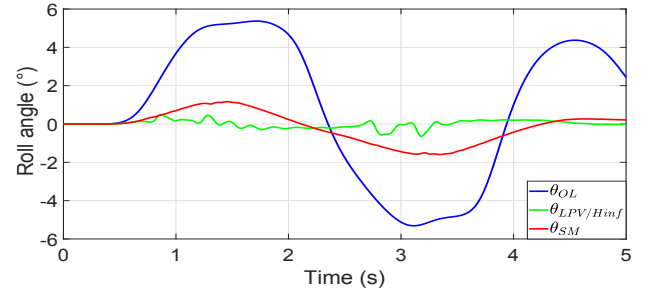Fig. 6. Yaw rate comparison
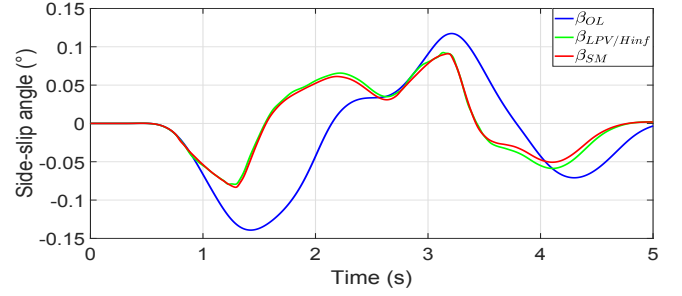
Fig. 7. Side-slip angle comparison

Fig. 8. Roll angle comparison

between $]0, 0.5]$.
The decision layer is the same as before to monitor the driver situation based on SI and LTR criteria, then it delivers the different gains λ_i in order to activate or deactivate the different actuators. These gains are given as follows (for more details see [Chokor et al. (2019)]):

$$\begin{aligned} \lambda_\beta &= \frac{1}{1 + e^{-\frac{8}{\overline{SI} - \underline{SI}}(SI - \frac{\overline{SI} + \underline{SI}}{2})}}, \\ \lambda_{\dot{\psi}} &= 1 - \lambda_\beta. \end{aligned} \qquad (35)$$

$$\lambda_\theta = \frac{1}{1 + e^{-\frac{8}{\overline{LTR} - \underline{LTR}}(LTR - \frac{\overline{LTR} + \underline{LTR}}{2})}}, \qquad (36)$$

Concerning the actuator layer, it is the same as the one was developed in the centralized architecture.

4. SIMULATION RESULTS

In this section, the developed controller will be validated with a double lane change test at 110 km/h as initial speed. All simulations are done using Matlab/Simulink with a complete nonlinear model of the vehicle [Chokor et al. (2016)], validated on "SCANeR Studio" (OKtal) [1] [Chokor et al. (2017)]. Then, a

---

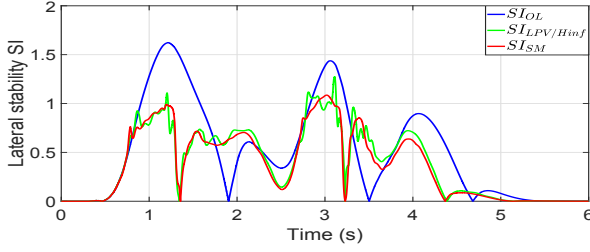[1] "SCANeR Studio" is a simulator dedicated to vehicle dynamics simulations.
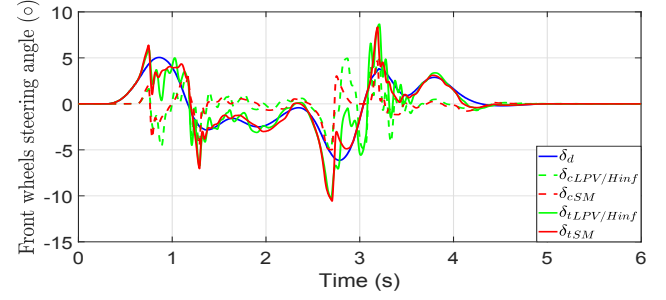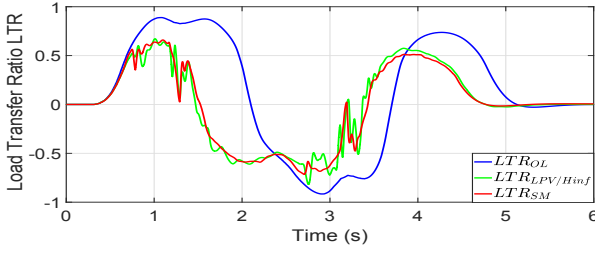
Fig. 9. Lateral stability comparison

Fig. 10. Load Transfer Ratio comparison
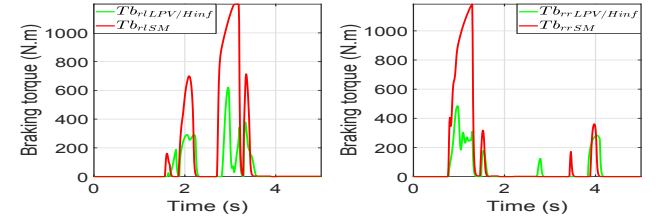
Fig. 11. Gains of $LPV/\mathscr{H}_\infty$ controller
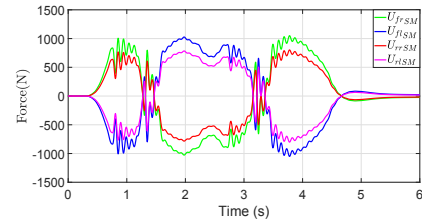
comparison is done between an uncontrolled vehicle, where no controller is used ("OL" as Open Loop) and controlled vehicle equipped with to different controllers, i.e, the centralized controller ("$LPV/\mathscr{H}_\infty$") and the decentralized one ("STSM" as Super-Twisting Sliding Mode). During this test, The driver's intention is to change the lane in a short time and then return to the same lane. Noting that in the two techniques of control, the active suspensions system AS aims to avoid rollover by decreasing the angle θ. But the validation of these controllers is done only on Matlab/Simulink because for this instant, the platform "SCANeR studio" simulator is not equipped with active suspensions system AS. The numerical values of the controller parameters used in the simulation are given in Table 2.

Fig. 6, 7 and 8 show the different control variables such as the yaw rate, the side-slip angle and the roll angle respectively. Fig. 6 shows that the yaw rate tracks the reference yaw rate delivered by the bicycle model, and both controllers have almost the same behavior compared with the uncontrolled vehicle. Thus, the maneuverability objective is achieved. In order to improve the lateral stability and to prevent an undesirable driver situation, the side-slip angle should be reduced as shown in Fig. 7. Both control architectures have similar influence on this angle. On the other hand, the convergence of roll angle to zero allows

Table 2. Controller Parameters for Simulation

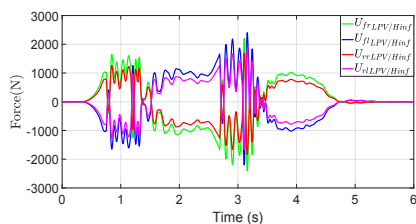| Parameters	Values
$M_1 = M_2 = M_3; T_1 = T_2 = T_3; \kappa$	$2; 0.1 = 10\%; 100$
$f_1 = f_2 = f_3; f_4; f_5 = f_6 = f_7$	$11.15\,Hz; 1\,Hz; 10\,Hz$
$c_1; c_2; r_1; r_2; r_3$	$9.55; 2.49; 2.5; 0.5; 0.1$
$\underline{SI}; \overline{SI}; \underline{LTR}; \overline{LTR}$	$0.6; 0.7; 0.6; 0.7$
$\delta_{c,max}^a; T_{b,max}^a$	$5°; 1200\,N.m$

Fig. 12. Steering angle comparison

Fig. 13. Braking comparison

Fig. 14. AS control inputs STSM controller

the avoidance of rollover risk, by reducing the load transfer ratio LTR. The Fig. 8 shows that the $LPV/\mathscr{H}_\infty$ controller is capable to diminish more the roll angle to zero compared to the STSM controller that is less performant w.r.t to $LPV/\mathscr{H}_\infty$ controller. Noting that the choice and the tuning of parameters ρ_1 and ρ_2 (Fig. 11) is not obvious since $LPV/\mathscr{H}_\infty$ controller aims to compromise between the different control objectives in order to give good results of optimality. For this reason, some oscillations appear in the Lateral stability index (Fig. 9) and the load transfer ratio (Fig. 10). Therefore, ρ_1 is chosen as $\rho_1 = \overline{\rho_1}$ when $SI \leq \underline{SI}$ in order to promote the maneuverability objective, while $\rho_1 = \underline{\rho_1}$ for a lateral stability improvement through the activation of differential braking actuators. Similarly, ρ_2 is chosen as $\rho_2 = \underline{\rho_2}$ almost all the time, except 1 s and 3 s, where LTR is less than $\underline{LTR} = 0.6$ and there is no risk of rollover. Around 1 s and 3 s, $\rho_2 = \overline{\rho_2}$ in order to increase the use of the active suspensions that diminish the roll angle, when the LTR becomes higher then the maximal threshold (see Fig.10).

Fig. 12 shows the driver steering angle δ_d, the AFS steering angle of both controllers δ_c and the total steering angle applied to the vehicle δ_t. The oscillations appear in δ_t with the $LPV/\mathscr{H}_\infty$ because the controller forced the maneuverability objective. Fig. 13 shows the differential braking torque of rear wheels. The decentralized controller activates more the braking to ameliorate the lateral stability, while the $LPV/\mathscr{H}_\infty$ saves energy. Fig. 14 and 15 show the AS control inputs of each controller. The vehicle speed is less dropped in the centralized approach since less braking is applied as can be seen from Fig. 16.

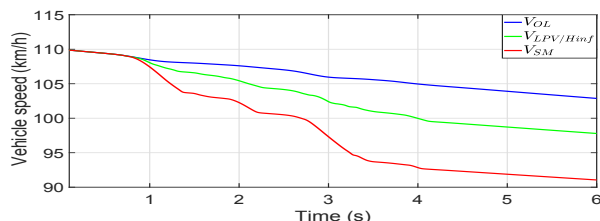Fig. 15. AS control inputs $LPV/\mathscr{H}_\infty$ controller

Fig. 16. Vehicle speed comparison

5. CONCLUSION AND PERSPECTIVES

To conclude, in this paper a centralized multilayer $LPV/\mathscr{H}_\infty$ control architecture has been developed to improve the overall vehicle performance. A coordination of the Active Front Steering, Direct Yaw Control and Active Suspensions in one centralized controller has been proposed, to enhance the global behavior of the system. The proposed controller is validated in Matlab/Simulink and a comparison is done with another decentralized approach based on the Super-Twisting Sliding Mode (STSM) technique. Results confirm the importance of active suspensions in the centralized approach to prevent the rollover risk. In the Future, the $LPV/\mathscr{H}_\infty$ controller will be extended, in order to realize more objectives concerning the vertical displacement, control of pitch-angle...with the introduction of artificial intelligence (AI)-based techniques to improve the decision layer and the tuning of gains, and to make the controller more robust and optimal. We will consider also the variation of the road adherence, and the generalization of centralized approach especially for tuning gains.

ACKNOWLEDGEMENTS

REFERENCES

Apkarian, P. and Gahinet, P. (1995). A convex characterization of gain-scheduled $\mathscr{H}_\infty$ controllers. *IEEE Transactions on Automatic Control*, 40(5), 853–864.

Apkarian, P., Gahinet, P., and Becker, G. (1995). Self-scheduled $\mathscr{H}_\infty$ control of linear parameter-varying systems: a design example. *Automatica*, 31(9), 1251–1261.

Chen, W., Xiao, H., Wang, Q., Zhao, L., and Zhu, M. (2016). *Integrated vehicle dynamics and control*. John Wiley & Sons.

Chokor, A., Talj, R., Doumiati, M., and Charara, A. (2019). A global chassis control system involving active suspensions, direct yaw control and active front steering. *IFAC-PapersOnLine*, 52(5), 444–451.

Chokor, A., Talj, R., Charara, A., Doumiati, M., and Rabhi, A. (2017). Rollover prevention using active suspension system. In *20th International Conference on Intelligent Transportation Systems (ITSC)*, 1706–1711. IEEE.

Chokor, A., Talj, R., Charara, A., Shraim, H., and Francis, C. (2016). Active suspension control to improve passengers comfort and vehicle's stability. In *19th International Conference on Intelligent Transportation Systems (ITSC)*, 296–301. IEEE.

Doumiati, M., Sename, O., Dugard, L., Martinez-Molina, J.J., Gaspar, P., and Szabo, Z. (2013). Integrated vehicle dynamics control via coordination of active front steering and rear braking. *European Journal of Control*, 19(2), 121–143.

Doumiati, M., Victorino, A., Talj, R., and Charara, A. (2014). Robust lpv control for vehicle steerability and lateral stability. In *53rd IEEE Conference on Decision and Control, pp. 4113–4118*.

Gu, D.W., Petkov, P., and Konstantinov, M.M. (2005). *Robust control design with MATLAB®*. Springer Science & Business Media.

He, J., Crolla, D.A., Levesley, M., and Manning, W. (2006). Coordination of active steering, driveline, and braking for integrated vehicle dynamics control. *Proceedings of the Institution of Mechanical Engineers, Part D: Journal of Automobile Engineering*, 220(10), 1401–1420.

Heißing, B. and Ersoy, M. (2010). *Chassis handbook: fundamentals, driving dynamics, components, mechatronics, perspectives*. Springer Science & Business Media.

Mirzaei, M. and Mirzaeinejad, H. (2017). Fuzzy scheduled optimal control of integrated vehicle braking and steering systems. *IEEE/ASME Transactions on Mechatronics*, 22(5), 2369–2379.

Poussot-Vassal, C., Sename, O., and Dugard, L. (2009). Robust vehicle dynamic stability controller involving steering and braking systems. In *IEEE European Control Conference (ECC)*, 3646–3651.

Rajamani, R. (2012). *Vehicle Dynamics and Control*. Springer.

Scherer, C., Gahinet, P., and Chilali, M. (1997). Multiobjective output-feedback control via lmi optimization. *IEEE Transactions on automatic control*, 42(7), 896–911.

Sename, O., Gaspar, P., and Bokor, J. (2013). *Robust control and linear parameter varying approaches: application to vehicle dynamics*. Springer, vol. 437.

Utkin, V. (2013). On convergence time and disturbance rejection of super-twisting control. *IEEE Transactions on Automatic Control*, 58(8), 2013–2017.

Vu, V.T., Sename, O., Dugard, L., and Gáspár, P. (2017). Enhancing roll stability of heavy vehicle by lqr active anti-roll bar control using electronic servo-valve hydraulic actuators. *Vehicle System Dynamics*, 55(9), 1405–1429.

Yao, J., Lv, G., Qv, M., Li, Z., Ren, S., and Taheri, S. (2017). Lateral stability control based on the roll moment distribution using a semiactive suspension. *Proceedings of the Institution of Mechanical Engineers, Part D: Journal of Automobile Engineering*, 231(12), 1627–1639.

Zin, A. (2005). *Sur la commande robuste de suspensions automobiles en vue du contrôle global de châssis*. Ph.D. thesis.